Downloaded from orbit.dtu.dk on: Nov 20, 2019

DTU Library

Wake modeling and simulation

Larsen, Gunner Chr.; Madsen Aagaard, Helge; Larsen, Torben J.; Troldborg, Niels

Publication date:
2008

Document Version
Publisher's PDF, also known as Version of record

Link back to DTU Orbit

Citation (APA):
Larsen, G. C., Madsen Aagaard, H., Larsen, T. J., & Troldborg, N. (2008). *Wake modeling and simulation*. Roskilde: Danmarks Tekniske Universitet, Risø Nationallaboratoriet for Bæredygtig Energi. Denmark. Forskningscenter Risoe. Risoe-R, No. 1653(EN)

General rights
Copyright and moral rights for the publications made accessible in the public portal are retained by the authors and/or other copyright owners and it is a condition of accessing publications that users recognise and abide by the legal requirements associated with these rights.

- Users may download and print one copy of any publication from the public portal for the purpose of private study or research.
- You may not further distribute the material or use it for any profit-making activity or commercial gain
- You may freely distribute the URL identifying the publication in the public portal

If you believe that this document breaches copyright please contact us providing details, and we will remove access to the work immediately and investigate your claim.

Risø DTU
National Laboratory
for Sustainable Energy

Wake modeling and simulation

Gunner C. Larsen, Helge Aa. Madsen, Torben J. Larsen, and Niels Troldborg

Risø-R-1653(EN)

Risø National Laboratory for
Sustainable Energy
Technical University of Denmark
Roskilde, Denmark
July 2008

Author: Gunner C. Larsen, Helge Aa. Madsen, Torben J. Larsen, and Niels Troldborg
Title: Wake modeling and simulation
Department: Wind Energy Division

Risø-R-1653(EN)
July 2008

Abstract (max. 2000 char.): We present a consistent, physically based theory for the wake meandering phenomenon, which we consider of crucial importance for the overall description of wind turbine loadings in wind farms. In its present version the model is confined to single wake situations. The model philosophy does, however, have the potential to include also mutual wake interaction phenomenons.

The basic conjecture behind the dynamic wake meandering (DWM) model is that wake transportation in the atmospheric boundary layer is driven by the large scale lateral- and vertical turbulence components. Based on this conjecture a stochastic model of the downstream *wake meandering* is formulated. In addition to the kinematic formulation of the dynamics of the "meandering frame of reference", models characterizing the *mean wake deficit* as well as the *added wake turbulence*, described in the meandering frame of reference, are an integrated part the DWM model complex. For design applications, the computational efficiency of wake deficit prediction is a key issue. A computationally low cost model is developed for this purpose. Likewise, the character of the added wake turbulence, generated by the up-stream turbine in the form of shed and trailed vorticity, has been approached by a simple semi-empirical model essentially based on an eddy viscosity philosophy.

Contrary to previous attempts to model wake loading, the DWM approach opens for a *unifying* description in the sense that turbine power- and load aspects can be treated simultaneously. This capability is a direct and attractive consequence of the model being based on the underlying physical process, and it potentially opens for *optimization* of wind farm topology, of wind farm operation as well as of control strategies for the individual turbine.

To establish an integrated modeling tool, the DWM methodology has been implemented in the aeroelastic code HAWC2, and example simulations of wake situations, from the small Tjæreborg wind farm, have been performed showing satisfactory agreement between predictions and measurements.

ISSN 0106-2840
ISBN 987-87-550-3693-2

Contract no.:
TREN07/FP6EN/S07.73680/038641

Group's own reg. no.:
1110062-01

Sponsorship:
European Commission in the framework of the NonNuclear Energy Programme Sixth Framework

Cover :

Pages: 28
Tables: 2
References: 13

Information Service Department
Risø National Laboratory for Sustainable Energy
Technical University of Denmark
P.O.Box 49
DK-4000 Roskilde
Denmark
Telephone +45 46774004
bibl@risoe.dk
Fax +45 46774013
www.risoe.dk

CONTENTS

Preface

This report constitutes part of the Work Package 4 reporting associated with the EU project “Next Generation Design Tool for Optimisation of Wind Farm Topology and Operation”. In Annex 1 to the contract of the aforementioned project, this report is denoted as deliverable D10. In addition to the present report, part of this work was presented at the EWEC’08 conference (cf. [2]).

1 Introduction

A *wake* is characterized by a mean wind decrease (i.e. wake deficit) and turbulence increase behind a turbine. The primary motivation for a detailed modeling of wind turbine wakes is that wind turbines located in wind farms experience inflow wind conditions that is substantially modified compared to the ambient wind field that apply for stand-alone wind turbines due to upstream emitted wakes. This drastic change of the environmental wind field conditions is caused by wakes emitted from upstream turbines, and it has implications not only for the power production of a wind farm, but also, and equally important, for the loading conditions of the individual turbines in the farm.

The downstream advection of a wake from the emitting turbine describes a stochastic pattern known as *wake meandering*. It appears as an *intermittent phenomenon*, where winds at downwind positions may be undisturbed for part of the time, but interrupted by episodes of intense turbulence and reduced mean velocity as the wake hits the observation point. Although different in nature compared to traditional turbulence, the resulting wind field may be considered as a turbulence field with intermittent characteristics, with a significantly modified turbulence *structure* and with increased "apparent" turbulence *intensity*. The notation "apparent" turbulence intensity indicates that the turbulence intensity contains contribution from both traditionally generated turbulence and from the wind speed variation caused by the instantaneous transversal- and vertical movements of the wake "emitted" from the upstream turbine.

A correct wind turbine load prediction requires both turbulence *intensity* and turbulence *structure* correctly described which is ensured by the Dynamic Wake Meandering (DWM) model complex. The approach taken in this model is believed to capture the essential physics of the wake problem, and it is completely different from traditional more empirically oriented approaches. Because the essential physics is captured, both load- and production aspects can be predicted, which is contrary to the traditional methods that typically focus on *either* load- *or* power prediction. As a consequence the proposed formulation opens for *optimization* of wind farm topology, of wind farm operation, as well as of control strategies for the individual turbine.

The approach taken in the DWM model complex is based on a *fundamental conjecture* stating that the transport of a wake in the atmospheric boundary layer can be modeled, as if the wake essentially acts as a passive tracer driven by the large-scale turbulence structures in the atmospheric boundary layer [1]. Following this philosophy, a simulation of the wind farm wind climate thus basically requires models of the (quasi-steady) wake deficit [2], the stochastic wake meandering process [1] and the added wake turbulence. The added wake turbulence concern small-scale turbulence with characteristic eddy sizes up to approximately one rotor diameter, and include contributions from conventional mechanically generated turbulence, caused by the shear associated with the wake deficit, as well as from the blade bound vorticity consisting mainly of tip and root vortices.

Apart from producing results that reflects the environmental reality for a wind turbine sited in wind farm conditions, the DWM model complex is straight forward to interface with existing state-of-the-art aeroelastic simulation packages [2]. This feature substantially eases the deployment/dissemination of the obtained results into the wind turbine community.

The present report offers a brief description of the DWM model, its implementation in the aeroelastic package HAWC2, and selected preliminary simulations of wake situations recorded at the Danish Tjæreborg wind farm. These simulations are subsequently compared with existing full-scale measurements of the wake flow field as well as of the turbine wake loading.

2 DWM model

The DWM model complex is basically constituted by three essential corner stones – namely a model of the quasi-steady *wake deficit*, a stochastic model of the down stream wake *meandering process* and, finally, a model of the added *wake turbulence*. The model complex is schematically illustrated in Figure 2-1.

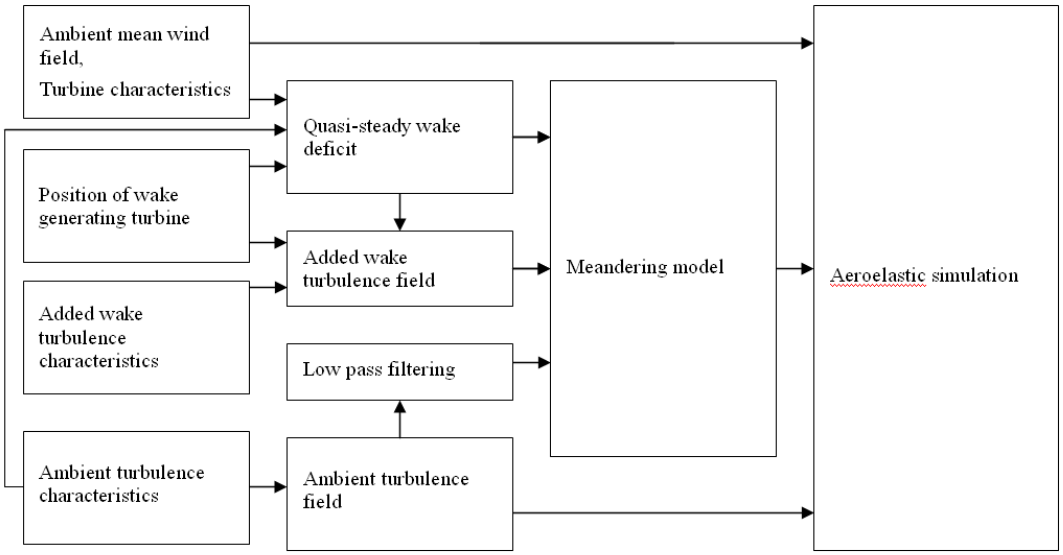

Figure 2-1 The main elements of the DWM model.

The *quasi-steady wake deficit* is the wake deficit formulated in the moving (meandering) frame of reference, and it includes the wake expansion as function of downstream transportation time caused partly by turbulence diffusion and partly by the rotor pressure field. The *wake meandering model* describes the stochastic downstream transport of the upstream emitted wakes driven by large scale turbulence structures, which are assumed not to be significantly affected by the presence a wind turbine. The *turbulence effects*, caused by an upstream located turbine, concern small-scale turbulence with characteristic eddy sizes up to approximately one rotor diameter and include contributions from conventional mechanically generated turbulence, caused by the wake shear, as well as from the blade bound vorticity consisting mainly of tip and root vortices. These vortices will initially take the form of organized coherent flow structures, but later, due to instability phenomena, gradually break down and approach the characteristics of conventional *isotropic in-homogeneous* turbulence with a length scale shorter than that of atmospheric turbulence [2], [3].

The involved sub-models are treated separately in the succeeding sub-sections along with a description of the integration of these models in the framework of the aeroelastic code HAWC2.

2.1 Quasi-steady wake deficit

The first version of the DWM model complex was based on quasi-steady wake deficits computed in a loop involving a coupling between an external CFD actuator disc model of the rotor-wake interaction and an aeroelastic model. However, in order to obtain a fully *integrated* formulation of the deficit prediction in the framework of the aeroelastic code HAWC2, the quasi-steady wake deficit prediction has been reformulated. The present formulation has three steps:

1. Initially, the "start" deficit - i.e. the deficit "emitted" from the upstream turbine - is determined by calculating the induced velocities in the rotor plane for the wake generating turbine in question.
2. Subsequently, the expansion of the computed rotor plane deficit in the near wake region is determined. This expansion is primary driven by the pressure recovery in the near wake regime.
3. Finally, the development (i.e. expansion and attenuation) of the wake deficit, as function of downstream distance from the wake generating turbine, is quantified taking into account the turbulent mixing caused by both ambient turbulence and by the turbulence generated by the wake shear field itself. This model is based on a thin shear layer approximation of the Navier-Stokes equations in their rotational symmetric form.

Step 1:

In a first approximation we assume *uniform inflow* conditions on the wake generating turbine – i.e. the effect of possible inflow wind shear profiles on the wake generation is excluded. This restriction is mainly introduced to match the description of the wake expansion described in item "Step 3", where rotationally symmetric[1] wake deficits also are assumed.

Based on the uniform inflow, induced velocities in annular rotor plane elements are calculated based on traditional Blade Element Momentum (BEM) theory. Blade pitch angles and rotor rotational speed are chosen to match the "*mean operational condition*" of the turbine in question at the selected wind speed.

Step 2:

The "initial" expansion of the wake, caused by the pressure rise in the *near wake region*, is calculated based on mass- and momentum balance considerations. Denoting the uniform rotor inflow wind speed by U_0 and the axial interference factor by a, the wake velocity along a stream line is reduced to $U_2 = U_0(1-2a)$ at down stream distances where the pressure loss has recovered, whereas the velocities at the rotor plane is reduced to $U_1 = U_0(1-a)$. In the present context we interpret the *near wake regime* as the regime extending from the rotor plane to the downstream distance where the pressure loss has recovered (i.e. typically the region within 2-3 rotor diameters downstream).

To match the BEM approach we assume that the above relations hold not only along a particular stream line, but also within annular stream tubes bounded by stream lines. Within this extension influence factors, characteristic for particular stream lines, are replaced with influence factors characteristic for particular stream tubes. Discretizing the radial coordinate in agreement with the BEM discretization (cf. Figure 2-2) the mass flow, $\dot{m}_i$, through the i^{th} annular stream tube, extending from $r_{t,i}$ to $r_{t,i+1}$ at the rotor plane and from $r_{w,i}$ to $r_{w,i+1}$ at the down stream border of the near wake regime, may be expressed as

$$\dot{m}_i = \rho\pi U_0\left(1-a_i\right)\left(r_{t,i+1}^2 - r_{t,i}^2\right),\ i = 1,\ldots,N-1 \tag{1}$$

and

$$\dot{m}_i = \rho\pi U_0\left(1-2a_i\right)\left(r_{w,i+1}^2 - r_{w,i}^2\right),\ i = 1,\ldots,N-1 \tag{2}$$

1 This symmetry restriction will be removed at a later stage, where the formulation of the wake expansion will be generalized from the present one dimensional formulation to a two dimensional formulation, and the present "Step 1" formulation thus generalized accordingly.

respectively, where N denotes the number of radial stations defined in the rotor plane. Assuming incompressibility, the continuity equation simply dictates the mass flows, expressed in equations (1) and (2), to be equal. This leads to an expression of the radius of the $(i+1)$'th far wake radius in terms of the *local* stream tube induction a_i, the i'th far wake radius and the i'th and $(i+1)$'th rotor radii, respectively. Consequently, we have the following simple iterative scheme for determination of the discretized radial coordinate in the wake at the down stream border of the near wake regime

$$r_{w,i+1} = \sqrt{\frac{1-a_i}{1-2a_i}\left(r_{t,i+1}^2 - r_{t,i}^2\right) + r_{w,i}^2} \ , \ i = 1,...,N-1 \tag{3}$$

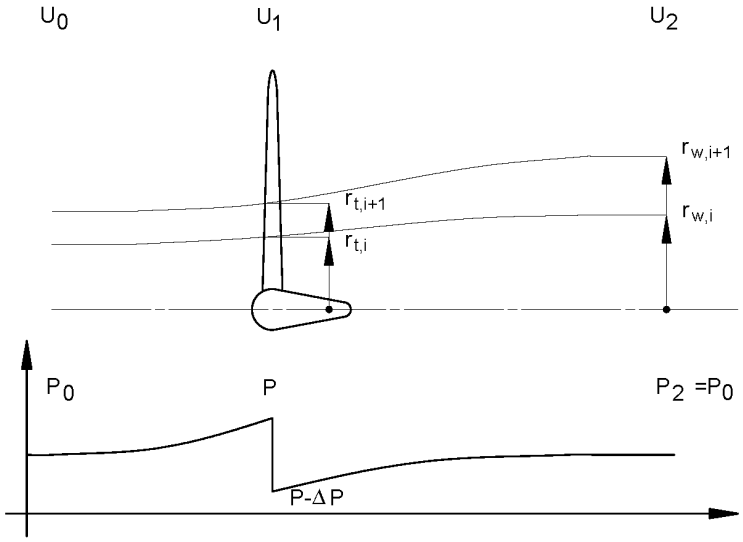

Figure 2-2: Wake expansion of an annular BEM stream tube due to pressure changes in the near wake region

A discrete representation of the wake deficit, U_w, as function of radial coordinate, at the down stream border of the near wake region, is thus finally defined as

$$U_w\left(\left(r_{w,i+1} + r_{w,i}\right)/2\right) = U_0\left(1-2a_i\right) \ , \ i = 0,...,N-1 \ , \tag{4}$$

where the average stream tube radius has been taken as the characteristic radial coordinate for the stream tube. With this approach, a supplementing radial coordinate is required to complete the downstream wake deficit description at the wake outer radius, where the flow velocity for continuity reasons has to take the value of the ambient flow

$$U_w\left(r_{w,N}\right) = U_0 \ . \tag{5}$$

The discretized wake representation defined by relations (4) and (5) is subsequently used as input to the modeling of the wake expansion further down stream as described in "Step 3". Note that flow velocities taking a uniform value, equal to the ambient flow velocity U_0, outside the wake outer radius is a simplification, since mass conservation implies higher flow velocities in the flow regime outside the wake. However, proper accounting of this feature requires (at least) a two dimensional modeling setup with e.g. a radial coordinate included in the flow equations.

Step 3:

The development of the wake deficit in the far wake regime (i.e. the down wind wake region extending beyond the near wake region) is mainly affected by turbulent mixing [3]. The present formulation of the model, handling the expansion caused by turbulent mixing, is strongly inspired by the work of Ainslie [4], [5], and [6].

We describe the turbulent mixing, occurring outside the near wake region, in terms of the rotationally symmetric Navier-Stokes equations with the pressure terms disregarded. Moreover, the gradients of mean flow quantities are assumed much bigger in radial direction (denoted by r) than in axial direction (denoted by x) which leads to the *thin shear layer approximation* of the rotationally symmetric Navier-Stokes equations. The momentum equation part of these equations may be expressed as

$$U\frac{\partial U}{\partial x}+V\frac{\partial U}{\partial r}=-\left(\frac{1}{r}\right)\frac{\partial}{\partial r}\left(r\overline{uv}\right), \tag{6}$$

where U and V denote the mean velocity in the axial- and radial directions, respectively, u and v denote the respective fluctuating velocity components in these directions, and an upper bar denotes temporal averaging.

Introducing the eddy viscosity concept, the Reynolds stresses are expressed as

$$-\overline{uv}=\upsilon_T\frac{\partial U}{\partial r}, \tag{7}$$

with the eddy viscosity given by

$$\upsilon_T(x)=l_m(x)U_m(x), \tag{8}$$

where U_m and l_m are suitable velocity- and length scales of the turbulence that in general will vary with the downstream distance x, but assumed *independent* of the radial coordinate r. The length- and velocity scales are taken to be proportional to the *instantaneous* wake half width, b, and the velocity difference, (U_0 - U_c), across the wake shear layer, respectively, where U_0 and U_c denote the ambient wind speed and the centre wake wind speed, respectively. Introducing equations (7) and (8) into equation (6), the governing momentum equation is reformulated as

$$U\frac{\partial U}{\partial x}+V\frac{\partial U}{\partial r}=\left(\frac{\upsilon_T}{r}\right)\frac{\partial}{\partial r}\left(r\frac{\partial U}{\partial r}\right), \tag{9}$$

with

$$\upsilon_T=k_1 b(U_0-U_c)+\upsilon_{TA}\ , \tag{10}$$

where k_1 is an empirical *constant* for the wake flow field. This empirical constant has been calibrated by comparing CFD actuator disc results, extracted from [3], with results predicted from the derived model, and the value $k_1 = 0.002$ seems to result in comparable predictions from the two models [2]. The second term in equation (10), υ_{TA}, is a viscosity term depending on the ambient turbulence level

$$\upsilon_{TA}=k_2 Ti \tag{11}$$

where k_2 is another empirical *constant*, and Ti is the turbulence intensity of the ambient turbulence. This constant has been calibrated by comparing predictions from the DWM model with predictions from a CFD actuator line model for the investigated turbine being in a partial wake loading condition [2]. With a selected value of $k_2 = 0.001$, the average levels of the root

mean square of the local inflow angle and the flapwise root bending moment, respectively, fits reasonably.

In addition to the momentum equation (9), the flow must fulfil the continuity equation given by

$$\frac{1}{r}\frac{\partial}{\partial r}(rV)+\frac{\partial U}{\partial x}=0 \tag{12}$$

The flow problem defined by equations (9) and (12) are solved using a finite difference scheme, with initial conditions defined by the down stream wake deficit obtained from the "Step 2" approach.

Example predictions of down stream wake deficits are shown in Figure 2-3 for a variety of down stream distances ranging between zero and ten rotor diameters. The example predictions refer to a 2MW NM80 turbine exposed to uniform turbulence free inflow conditions with mean wind speed equal to 5.75m/s. Notable is the significant effect on the wake deficit arising from the pressure loss recovery in the near wake regime, and the gradually attenuation and expansion of the quasi-steady wake deficit taking place for increasing downstream distances within the far wake regime.

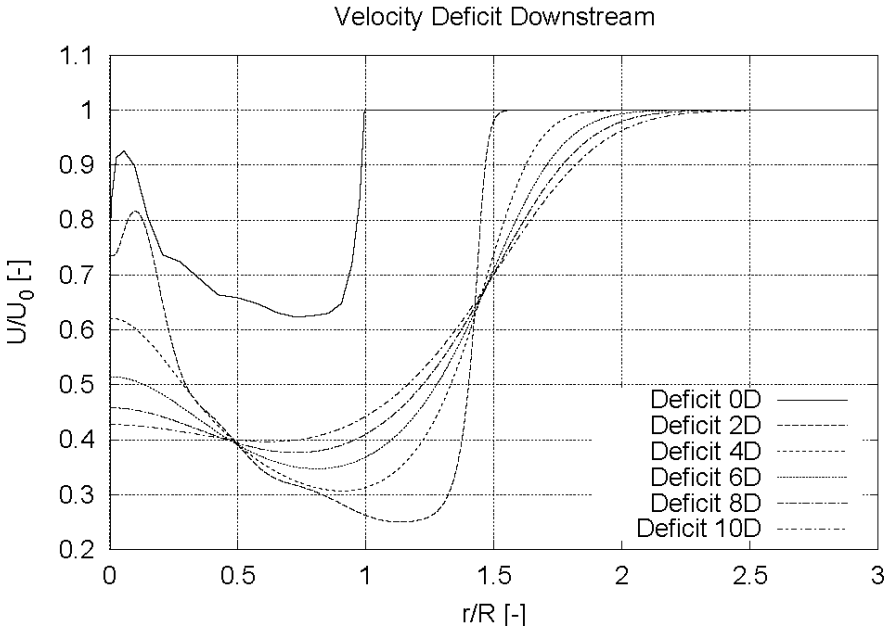

Figure 2-3: Final deficit at selected downstream distances including pressure expansion from 0D to 2D and turbulent mixing (using $k_1 = 0.002$*) further downstream.*

2.2 **Added wake turbulence**

We denote the total intermittent wake turbulence as *apparent turbulence*. The apparent wake turbulence contains contributions from both the meandering of the quasi-steady wake deficit and from so-called *added wake turbulence.* The added wake turbulence include contributions from conventional mechanically generated turbulence, caused by the *wake shear*, as well as from the *blade bound vorticity*, consisting mainly of tip and root vortices. The tip vortices will initially take the form of organized coherent flow structures, but later, due to instability phenomenon's, gradually break down and approach the characteristics of conventional turbulence – although with modified turbulence characteristics compared to atmospheric turbulence. In analogy with the description of the wake deficit, we aim at a description of the added wake turbulence in the meandering frame of reference.

Whereas the meandering of the wake deficit primary adds to the low frequency part of the apparent turbulence spectrum, the added wake turbulence primary adds to the high frequency part of this spectrum. Compared to conventional atmospheric turbulence, the added wake turbulence is characterized by being both *in-stationary* (develops with the downstream transportation time) and *inhomogeneous* (vary in general across the wake regime). In addition, the wake turbulence tends to be *more isotropic* and displays *increased turbulence standard deviation* and *reduced turbulence length scale*. The high-frequency part of the spectra follows the inertial sub-range law, but with higher dissipation rate than in the ambient turbulence case.

We have approached the description of added wake turbulence in two ways – a crude and a more elaborate consistent approach. Presently, only the crude approach is fully implemented in the DWM model. However, essential sub-models for the more consistent model have been formulated.

Crude approach

In the crude approach the added *in-homogeneous* wake turbulence, at a particular downstream position, is modeled based a *homogeneous* Mann turbulence field [7] with cross sections of the turbulence box covering 1 rotor diameter. The turbulence length scale is short – i.e. of the order of 1.5 times the diameter of the wake generating rotor [3] – and the mutual ratio between variance of the longitudinal (u), transversal (v) and vertical (w) turbulence components is equal to 1.0 corresponding to isotropic turbulence. The resolution of the turbulence box is high (i.e. 128×128 points) in planes perpendicular to the mean flow direction to allow small turbulence eddies to be resolved reasonably well. The length of the turbulence box in the mean flow direction is 2.5 rotor diameters with a resolution of 128 points. Turbulence is re-used[2] when points outside the box are requested – i.e. when longer time series are required for the aeroelastic load simulation.

The added turbulence refer to the meandering frame of reference, and the (v,w) centre position of the turbulence box thus follows the centre position of the associated wake deficits.

Although violating the second order statistics of the turbulence field, the *in-homogeneity* of the added turbulence is approximated by *simple scaling* of the created homogeneous Mann field. *Rotationally symmetry* of added wake turbulence intensity is assumed, resulting in a scaling coefficient depending on the radial rotor coordinate only. The selected scaling factor, k_{mt}, depends on the quasi-steady *deficit depth*, U_{def}, at the considered down stream distance, as well as on the *deficit gradient*, $\frac{\partial U_{def}}{\partial r}$, according to equation (13).

$$k_{mt}(r) = \left|1 - U_{def}(r)\right| k_{m1} + \left|\frac{\partial U_{def}(r)}{\partial r}\right| k_{m2} \tag{13}$$

Two empirical factors k_{m1} and k_{m2} are introduced to schedule the gain of these two contributions. The two factors have been tuned by comparing predictions from the DWM model with predictions from a CFD actuator line model for the investigated turbine being in a partial wake loading condition [2]. A good agreement between predictions from the two models, in terms of root mean squares of the local inflow angle, the local relative velocity and the flapwise root bending moment, respectively, is obtained selecting $k_{m1} = 0.6$ and $k_{m2} = 0.25$. Typically qualitative appearances of respectively the deficit depth shape function and the gradient deficit shape function are shown in Figure 2-4.

2 This approach is justified by the fact that the length scale of the added turbulence is small, and consequently that the correlation between turbulence components separated more that 2.5 rotor diameters is modest.

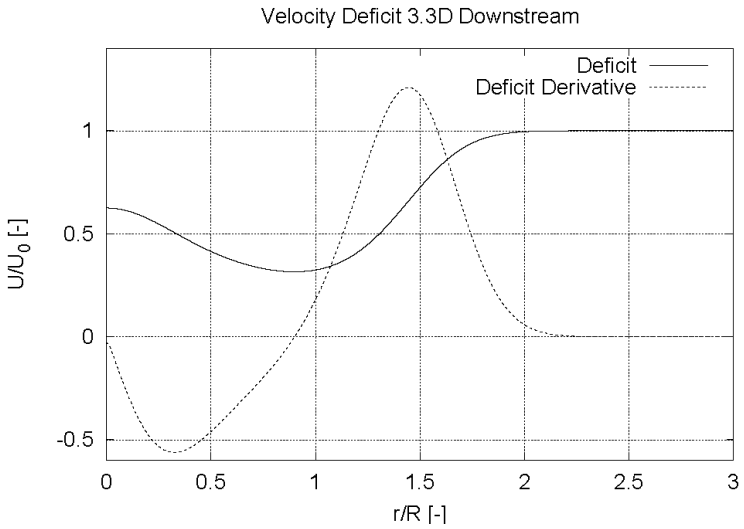

Figure 2-4: Deficit and radial derivative of deficit used for micro turbulence scaling.

Consistent approach

The basic philosophy behind the consistent approach is to characterize the in-homogeneous added wake turbulence field, at a particular down stream position, in terms of in-homogeneous variance, in-homogeneous length scale, and coherence turbulence properties depending on the spatial position(s) within the wake. In a simplifying approach *rotational symmetry* is assumed, thus essentially neglecting the effect on added turbulence originating from a possible mean shear of the inflow on the wake generating turbine. Having defined the in-homogeneous turbulence characteristics, these are subsequently used as input to a turbulence generator, capable of handling inhomogeneous turbulence properties, to generate the requested turbulence field.

Two paths will be pursued in TOPFARM to characterize the in-homogeneity of the added wake turbulence – one based on numerical CFD studies performed in Work Package 1, and the other based on detailed experimental studies performed in Work Package 4 using a newly developed 2D LiDAR technology [8] combined with pitot tube sensor recordings.

In the following a preliminary *qualitative characterization* of the added wake turbulence, based on CFD actuator line (ACL) simulations, will be outlined based on an inflow field *without* ambient turbulence. For real wind farm situations, the wake turbulence, in the meandering frame of reference, consists of contributions from both the ambient turbulence and the added wake turbulence. The basic idea behind the simulation based on a *turbulence free* inflow field is to "separate" the added wake turbulence in the wake flow field from the turbulence contribution caused by the ambient turbulence. However, at least in the near wake, these contributions are de facto *not* independent, as the ambient turbulence will contribute to a faster break down of organized wake structures consisting mainly of tip- and root vortices (i.e. accelerate the process of these structures becoming instable). Nevertheless, the analysis is believed to contribute to the qualitative characterization of the wake added turbulence when fully developed.

The analysis is based on the flow conditions at the downstream distance where the added wake turbulence are *just* fully developed (i.e. the smallest possible downstream distance where the added wake turbulence are fully developed). The simulation refers to a 2MW turbine with a rotor diameter equal to 80m, and an inflow shear corresponding to a shear coefficient equal to 0.2 in a power law profile given by

$$U = U_0\left(\frac{z}{H}\right)^{\alpha}, \qquad (14)$$

where H denotes the reference height (here chosen as one rotor diameter), and z is the height above terrain. The rotational speed of the rotor is 12.1RPM, U_0 = 5m/s, and the rotor thrust coefficient is equal to 0.87.

To comply with the requirement of fully developed added wake turbulence (for the selected mean wind speed), we have selected a flow cross section positioned 14 rotor radii (R) downstream for this analysis. In subsequent analyses more down stream distances, as well as more mean wind speeds, will be included to construct a more complete picture of added wake turbulence characteristics, and to relate these to basic operational turbine characteristics. The present analysis is based on a 26.5 minute long ACL simulation.

In a first order approach, we will take the simplifying approach of *rotationally symmetry* of the wake turbulence, although asymmetries in the aerodynamic induction of the wake generating upstream turbine, caused by mean wind shear and turbine tilt, to some degree may violate this assumption. The assumed rotationally symmetry of the wake turbulence allow us to replace conventional *spectral averaging*, based on data segmentation, with an averaging procedure based on azimuthal averaging for a given radial position. With this approach, the low frequency part of the spectrum is conserved. The highest frequency resolved corresponds to the smallest distance resolved (i.e. the grid cell size). We have analyzed azimuthally averaged spectra associated with 4 different radial positions – 0.25R, 0.5R, 0.75R and 1R. Normalized results are shown in Figure 2-5 – Figure 2-7 for the streamwise-, the transversal- and the vertical turbulence components, respectively.

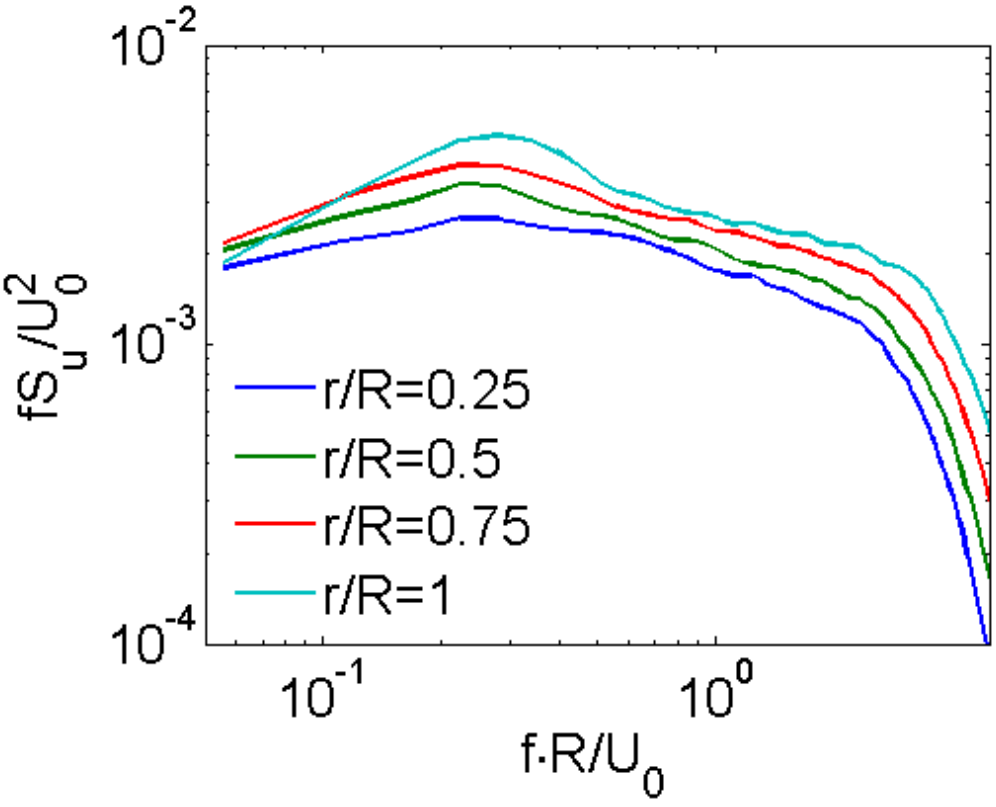

Figure 2-5 Spectra of the u-turbulence component at different radial positions 14 R downstream.

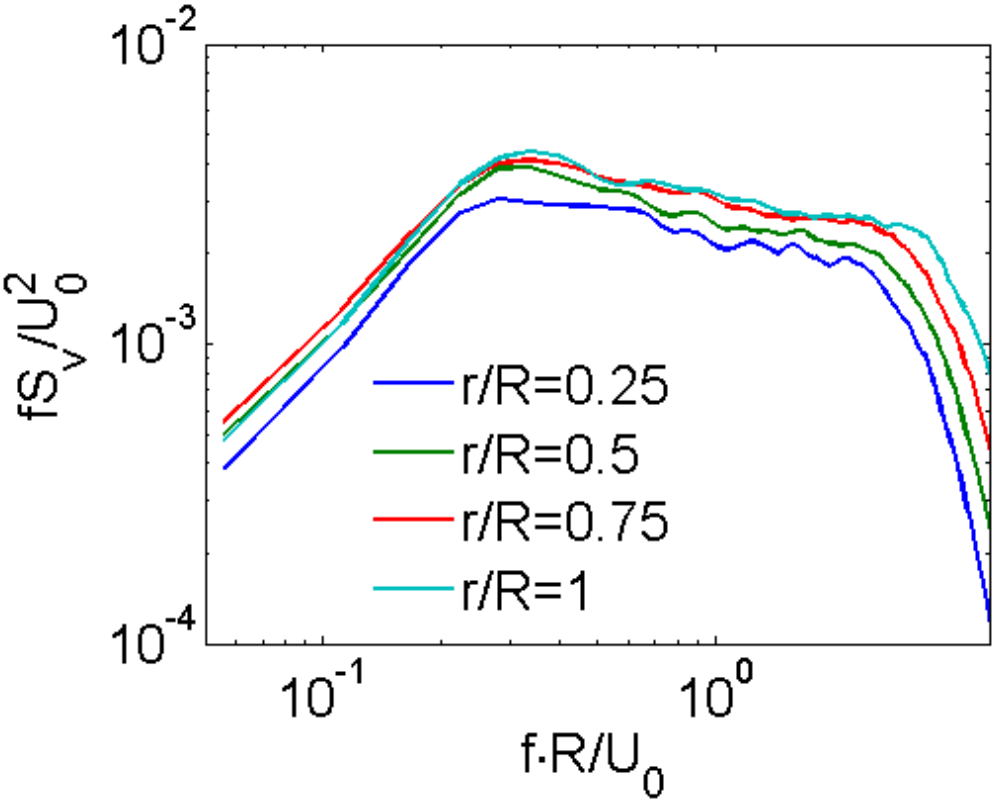

Figure 2-6 Spectra of the v-turbulence component at different radial positions 14 R downstream.

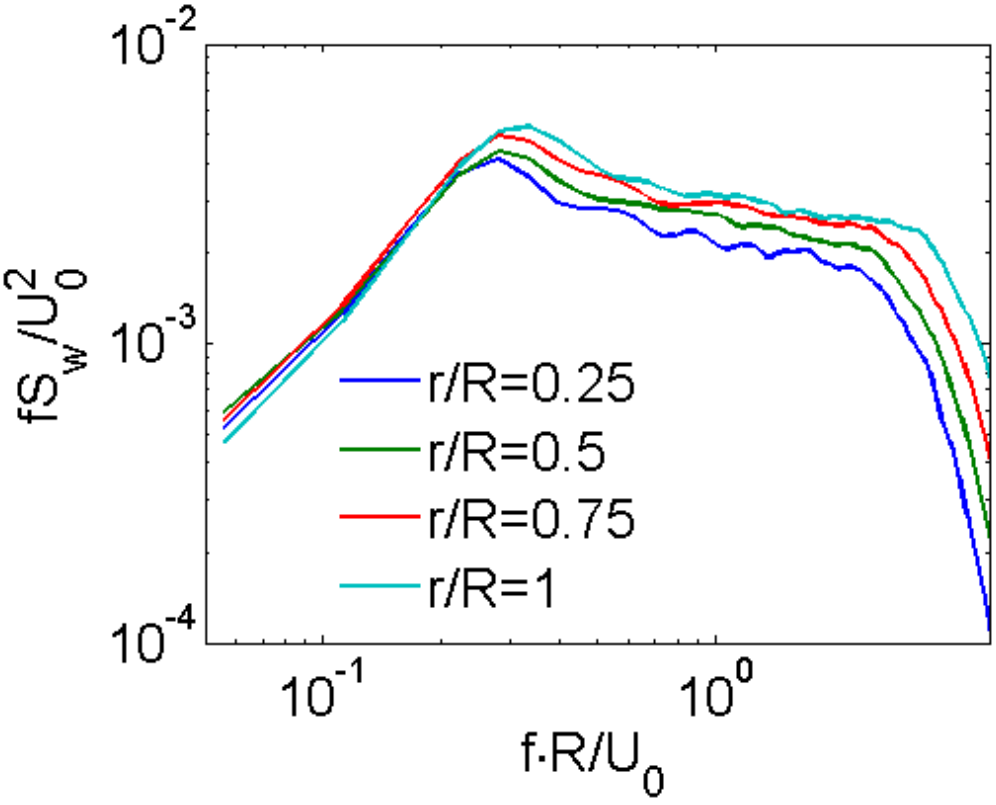

Figure 2-7 Spectra of the w-turbulence component at different radial positions 14 R downstream.

The spectra is typically composed of an *energy-containing sub-range* characterized by low frequency components of limited statistical significance, an *inertial sub-range* with a spectral gradient close to –2/3 in agreement with the theoretical expectation, and a *dissipation sub-range* which, in the case of these numerically based spectra, is resulting from the limited spatial resolution as well as from numerical diffusion.

It is characteristic that the turbulence has the largest content of energy in the annular wake segment associated with the highest gradient of the wake deficit (cf. Table 2-1), although not as pronounced as reported in [3]. This feature is also reflected in the crude formulation of the wake turbulence model (cf. equation (13)).

The degree of isotropy of wake added turbulence is enlightened by computing the *turbulent energy*, expressed in terms of root mean square, and the *turbulence length scales* for the 3 turbulence components at the investigated radial positions. For definition of the length scale, we will use the (one-sided) Kaimal spectrum as the generic spectrum to which the observed spectra will be fitted, thus following the procedure outlined in [3]. The results are summarized in Table 2-1 and Table 2-2, respectively.

	σ_u/U_0 $[m^2/s^2]$	σ_v/U_0 $[m^2/s^2]$	σ_w/U_0 $[m^2/s^2]$
0.25R	0.108	0.112	0.117
0.50R	0.120	0.123	0.125
0.75R	0.130	0.130	0.133
1.00R	0.139	0.133	0.138

Table 2-1 Root mean square of turbulence components at different radial positions.

	L_u /R	L_v /R	L_w /R
0.25R	1.16	0.27	0.33
0.50R	1.06	0.27	0.30
0.75R	0.93	0.26	0.27
1.00R	0.65	0.23	0.24

Table 2-2 Turbulence length scale of various turbulence components at different radial positions.

As seen the *degree of isotropy*, quantified in terms of root mean square of the added wake turbulence, is close to perfect for the investigated radial positions. For the quantification in terms of length scale, however, isotropic characteristics are only obtained for the lateral- and vertical turbulence components, respectively. For ideal isotropic turbulence, the turbulence length scales associated with the lateral and vertical turbulence components should be identical [9], which is clearly demonstrated for the computed turbulence. The turbulence scale associated with the longitudinal turbulence component, however, should be of the order 1.45 times the other two length scales for homogeneous turbulence [9]. This is not reflected in the computed wake added turbulence, where this factor varies in the range 2.7-4.3. A possible explanation is the lack of homogeneity of the analyzed wake turbulence.

Finally, the wake *coherence properties* have been extracted from the numerical investigations. The assumed *rotational symmetry* of the wake statistics results in a substantial reduction in the parameterization of the coherence as compared to the general inhomogeneous case.

The spectral coherence, Γ, may be defined as

$$\Gamma = \frac{\left|S_{ij}(f)\right|^2}{S_{ii}(f)S_{jj}(f)} \tag{15}$$

where f is frequency, S_{ij} is the cross-spectra between two points identified by "*i*" and "*j*", respectively, and S_{ii} and S_{jj} is the analogue auto-spectra.

Since wake turbulence is *spatially inhomogeneous*, the coherence will vary with the position of the involved points. The coherence properties of a spatial inhomogeneous turbulence field are in general governed by 7 parameters (3 spatial coordinates for each point and the frequency). However, because the turbulence field in the present case is assumed *rotational symmetric* in a statistical sense, the number of required independent parameters can be reduced to 3 geometric parameters and the frequency parameter. Considering the *spatial distance* between the points as the most essential spatial parameter, the spectral coherence between two points may be parametrized as

$$\Gamma = \Gamma\left(r_m, \varphi, d_{ij}, f\right) \tag{16}$$

where r_m denotes the mean radial distance of the two points, d_{ij} is the distance between the two points, and the angle φ is defined in Figure 2-8.

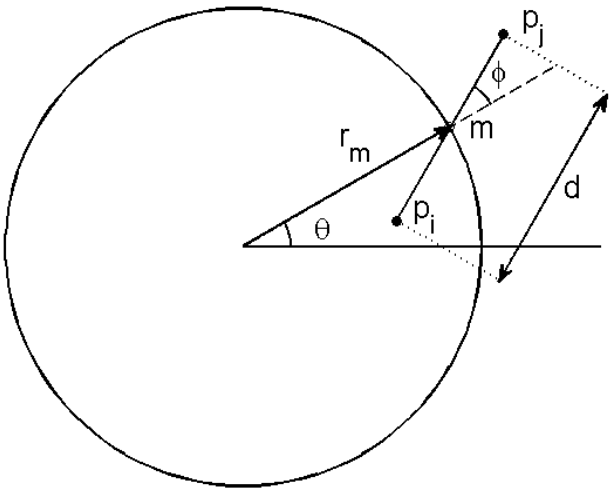

Figure 2-8 Coherence parameter definitions.

Because of the assumed rotational symmetry, it suffices to restrict φ to the interval $[0; \pi/2]$.

In analogy with conventional parametrization of coherence in the atmospheric boundary layer, we assume the added wake coherence properties to be governed by the following exponential behavior

$$\Gamma = Exp\left(-C\left(r_m, \varphi\right)\frac{f\,d}{U_0}\right) \tag{17}$$

where $C(r_m,\varphi)$ is a *coherence decay function*. Adopting this formulation, the coherence, for fixed values of r_m and φ, should be invariant changes in frequency and displacement as long as the

product of these parameters is kept constant. This has been investigated in [10], where the coherence, for fixed values of r_m and φ, were shown approximately to collapse to a single curve when plotted against the reduced frequency for various displacements.

For the selected flow cross section, the coherence decay function, $C(r_m,\varphi)$, is determined by performing a least-square fit of equation (16) to the curve obtained by averaging coherence curves representing various displacements. The resulting decay function is shown in Figure 2-9.

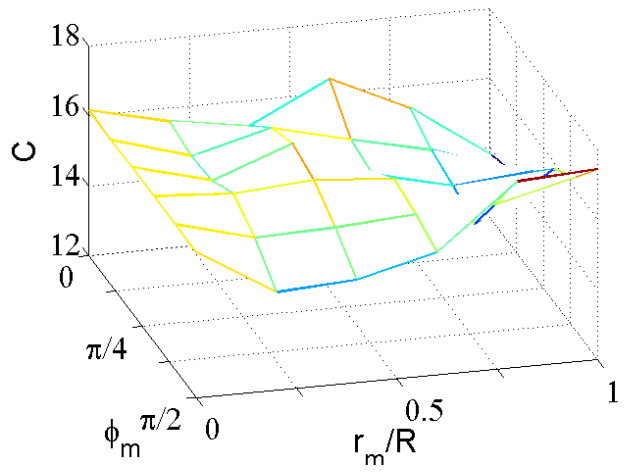

Figure 2-9 Computed coherence decay function.

The coherence decay of the added wake turbulence is generally increased significantly compared to the coherence decay observed for conventional homogeneous atmospheric turbulence. Moreover, non-constant character of $C(r_m,\varphi)$ reflects the in-homogeneous nature of the wake turbulence.

With the added wake turbulence characteristics in hand, the final step is to simulate a turbulence field with these characteristics. Suitable algorithms for this purpose are already available [11]. These algorithms are based on the Shinozuka approach [12], [13] which, contrary to the Mann algorithm [7], are based on one-point (auto-)spectra and two-point cross-spectra that may *vary in space*.

The Mann spectral method combines Rapid Distortion Theory, an assumed linear mean wind shear, the Von Kármán spectral tensor and a model for eddy lifetime, and it is restricted to homogeneous Gaussian turbulence fields. Although the spectral tensor in principle contains the same information as the cross spectra, the tensor formulation leads to considerable simpler and faster simulations of turbulence than the cross spectra based methods. This type of synthetic turbulence field generation will therefore still be used for simulating the *ambient turbulence field* as well as the large scale turbulence field applied for the description of the meandering process (cf. Section 2.3).

Basically, the Shinozuka algorithm produces a multitude of correlated stochastic time series referring to pre-selected points in space based on multivariate Fourier simulation. The general idea of multivariate Fourier simulation is first to generate Fourier components with proper statistics (that may vary in space) and subsequently convert them into time series by inverse FFT. This procedure is a *linear* combination of stochastic variables, and the result will thus remain Gaussian if the input is. The correlation matrices of the Fourier components are known to be Hermite symmetric, which can be "square-root" factorized by applying Choleski decomposition. Gaussian

Fourier components with prescribed correlation is generated from a vector of random independent complex Gaussian variables and multiplied by this "square-root" matrix. The frequency dependence is usually quite smooth, and it is therefore often a good approximation to perform the computationally expensive Choleski decomposition at a reduced set of frequencies, and subsequently interpolate between these.

2.3 Wake meandering

The wake meandering part is based on a *fundamental presumption* stating that the transport of wakes in the atmospheric boundary layer can be modeled by considering the wakes to act as *passive tracers* driven by the *large-scale* turbulence structures. Modeling of the meandering process consequently includes considerations of a suitable description of the "carrier" stochastic transport media as well as of a suitable definition of the cut-off frequency defining large-scale turbulence structures in this context.

For the stochastic modeling of wake meandering, we imagine a wake as constituted by a *cascade* of wake deficits, each "emitted" at consecutive time instants in agreement with the passive tracer analogy [1], [3]. We then subsequently describe the propagation of *each* of the "emitted" wake deficit, and the collective description of these thus constitutes the wake meandering model.

Adopting Taylor's hypothesis, the *downstream advection* of these is assumed to be controlled by the mean wind speed of the ambient wind field. With this formulation the wake momentum in the direction of the mean flow is invariant with respect to the prescribed longitudinal wake displacement. This is a considerable simplification allowing for a straight forward decoupling of the wake along wind deficit profile (and its expansion) and the wake transportation process.

As for the dynamics in the *lateral- and vertical directions*, each considered wake cascade-element is displaced according to the large-scale lateral- and vertical turbulence velocities at the position of the particular wake cascade element at each time instant.

In mathematical terms, the wake deficit dynamics in the lateral direction, y, and the vertical direction, z, is thus assumed described by the following differential equation system

$$\frac{dy(t,t_0)}{dt} = v_c(y,z,t,t_0) \ , \tag{18}$$

$$\frac{dz(t,t_0)}{dt} = w_c(y,z,t,t_0) \ , \tag{19}$$

where v_c and w_c are the spatially dependent large-scale turbulent velocities, and t_0 denotes the time instant at which the considered cascade element is emitted.

The choice of a suitable stochastic turbulence field, that in turn defines the stochastic wake transport process, is not mandatory, but may be guided by the characteristics of the atmospheric turbulence at the site of relevance. These characteristics encompass in principle not only turbulence standard parameters such as turbulence intensity, turbulence length scale and coherence properties, but also features like degree of isotropy, homogeneity of the turbulence, Gaussianity of the turbulence etc..

The fundamentals of the DWM model has been preliminary verified by correlating DWM predictions with full-scale measurements of the instantaneous wake position obtained from LiDAR recordings [8].

2.4 Implementation in HAWC2

The DWM model has been integrated in the aeroelastic package HAWC2. The implementation offers the possibility of dealing with *several wake sources* simultaneously, which is especially useful for simulations of turbines in wind farms with more than one neighboring turbine present. The turbines are assumed to have identical aeroelastic properties, and presently only situations where a particular turbine is affected by independent single wakes can be dealt with. In the future, however, additional facilities for modeling of merging wakes will be developed and included.

The DWM model implementation consists of the following 3 steps, where the first 2 steps are calculated initially:

1. Calculation of the deficits, as function of downstream distance from the wake generating turbines, according to the procedure outlined in Section 2.1;
2. Determine the stochastic wake meandering processes for the involved turbines as a cascade of "emitted" wake deficits as described in Section 2.3.
3. For each wake deficit the wake generated small scale turbulence, as described in Section 2.2, is added to the ambient turbulence in the relevant deficit region.

The turbulence field chosen as the stochastic transport media generating the wake meandering is the Mann turbulence model [1], since this turbulence field is fully correlated between *u*, *v* and *w*, formulated in Cartesian coordinates, and further enables unequal grid resolution and size in the three directions, see Figure 2-10.

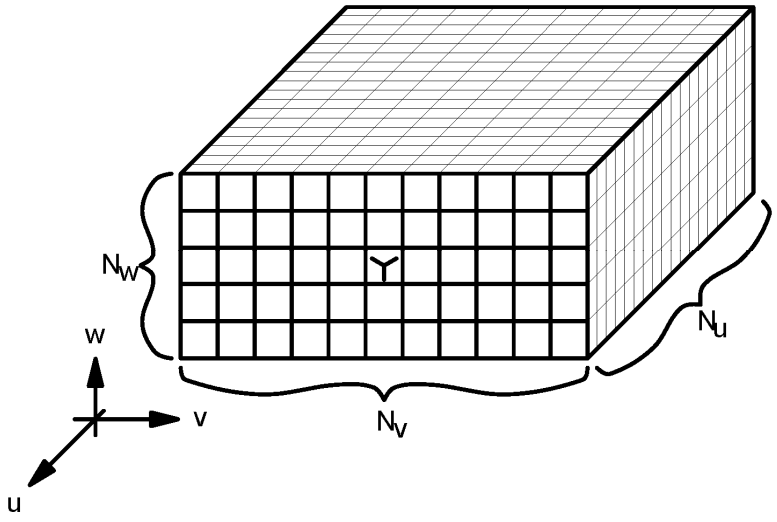

Figure 2-10 Mann turbulence box layout for the meander turbulence. A course grid resolution (size of 1 rotor diameter) is seen in the in-plane v,w direction, whereas the resolution in the u-direction is chosen to be fine.

A course grid resolution is chosen in the in-plane direction since this first of all enables an effective cut-off frequency filtering neglecting all eddies with a size less than the rotor, secondly to enable very large spatial dimensions of the box which is especially important if several wake sources are considered. A special feature when using several upstream wake sources in the same turbulence field is that if a wake passes the centre of the next turbine, the two wakes will remain together for the rest of the transport since they meet the same turbulence. The grid resolution in the *u*-direction is chosen with a finer resolution in order to get a smooth continuous variation in

deficit centre positions. It is important that the grid point velocities represent the mean value of a grid cube in order to provide a correct spatial filtering.

3 Results

Selected characteristics of predictions from the DWM model implementation, described in Section 2.4, are compared with existing full-scale experimental data obtained from a 2MW wake operating turbine at the Tjaereborg wind farm in Denmark. This turbine is identical to the turbine applied for the comparative study of the ACL and DWM models in [2], which subsequently resulted in the selected values of both the parameters defining the eddy viscosity in the wake expansion model (cf. Section 2.1), and the parameters in the model for the added wake turbulence (cf. Section 2.2).

3.1 Full-scale experimental data

The selected characteristics encompass *wake flow field characteristics*, as measured directly in the rotor plane of the wake operating turbine, and induced *structural response characteristics* in the form of blade root moments. The blade root moments are established by standard strain-gauge recordings, whereas the flow field observations are based on an experimental setup using a five hole pitot tube mounted at the blade leading edge in radius 24m.

From the five hole pitot tube measurements the *local inflow angle*, in the plane perpendicular to the blade span, can be derived and likewise the *local, relative velocity*. Due to the geometrical conditions for the local inflow velocity vector, the relative velocity signal will mainly show the characteristics of the two lateral turbulence components, whereas the local inflow angle mainly reflects the characteristics of the longitudinal turbulence component. The measured inflow angle was corrected for upwash from the bound circulation on the blade section at the pitot tube position, whereas no corrections were applied to the measured relative velocity.

As the focus of the present analysis is characteristics of the *wake turbulence*, the existing data base was searched for inflow conditions with *low ambient turbulence*, as low ambient turbulence implies only modest meandering of the wake, thus minimizing the effect from meandering in the measured turbulence characteristics. A few data files with such conditions (turbulence intensity around 3%) were found, and three 10 min. data files, measured within one hour, were selected since they contained both free inflow and wake conditions for an upstream turbine in a distance of 3.5 D. Unfortunately, meteorological conditions with low ambient turbulence are often associated with a strong wind shear and a change of wind direction as function of height. This is also the case for the three selected data files, but the inflow conditions in the models were adapted to give an optimal correlation between simulated and measured local in-flow angle, local relative velocity and flap-wise moment, binned in the azimuthal coordinate. The wind shear was modeled with an exponential curve with an exponent of 0.7, and a yaw error of 15 degree was applied. The relative velocity binned in the azimuthal coordinate provides an excellent basis for adjusting the yaw error to the measured data.

3.2 Simulations

The DWM model is run to simulate specific wake conditions, defined by the three 10 min. experimental data files which have been selected for the mutual comparison of numerical predictions and measured data in Section 3.1. In all three simulations the strong wind shear observed in the measurements are applied. Comparative results for statistics of the wake flow field (local inflow angle, local relative velocity) and the structural response (flapwise root bending moment) are shown in Figure 3-1, Figure 3-2 and Figure 3-3, respectively. Also included is a

comparison of rainflow counting results associated with the flapwise root moment. These results are shown in Figure 3-4.

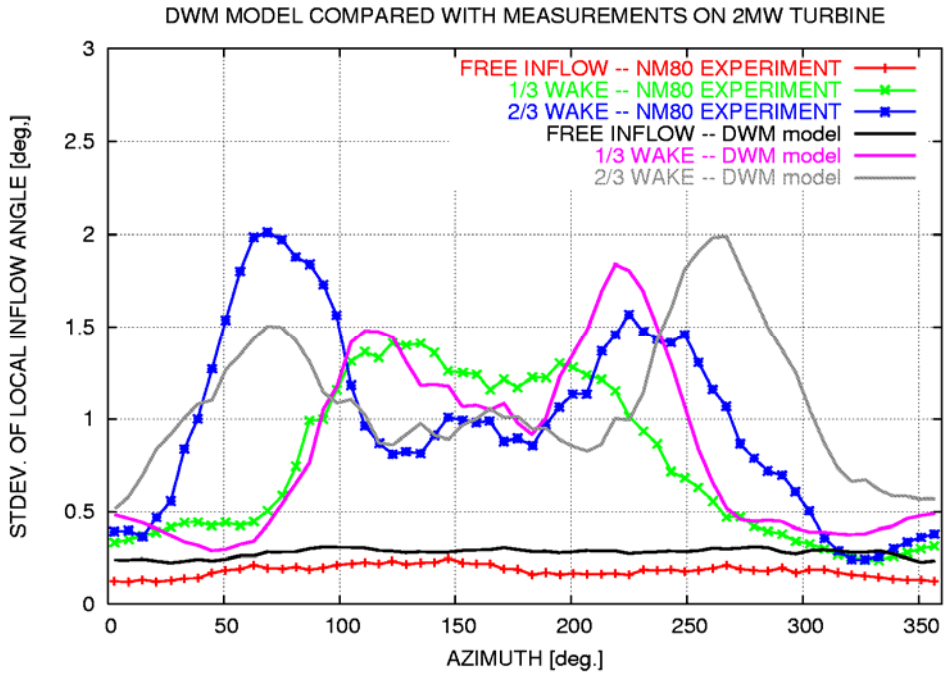

Figure 3-1 Comparison of root mean squares of the local inflow angle as simulated with the DWM model and obtained from full scale measurements, respectively.

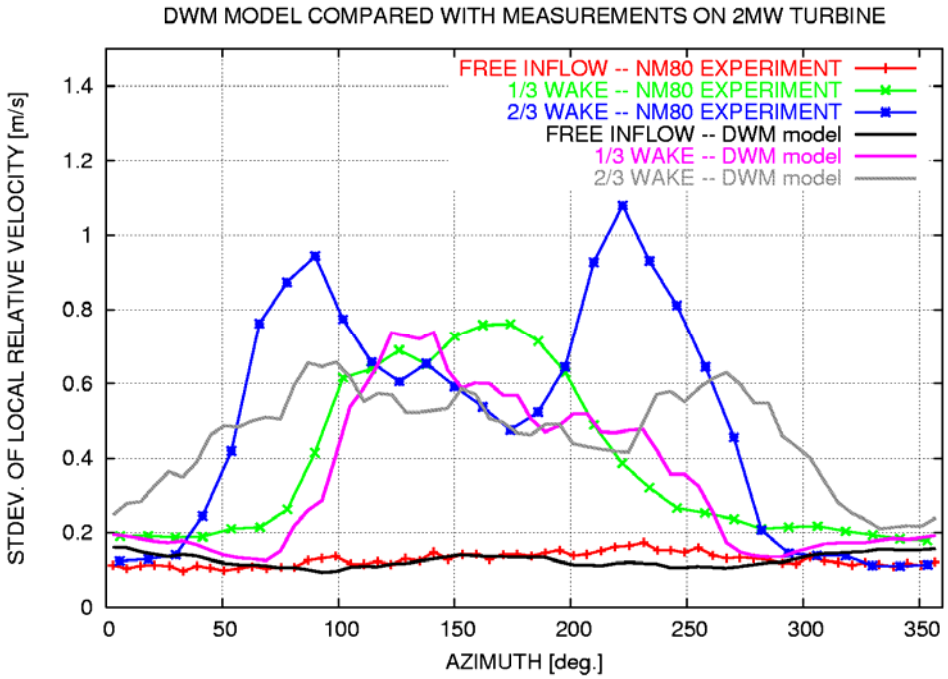

Figure 3-2 Comparison of root mean squares of the local relative velocity as simulated with the DWM model and obtained from full scale measurements, respectively.

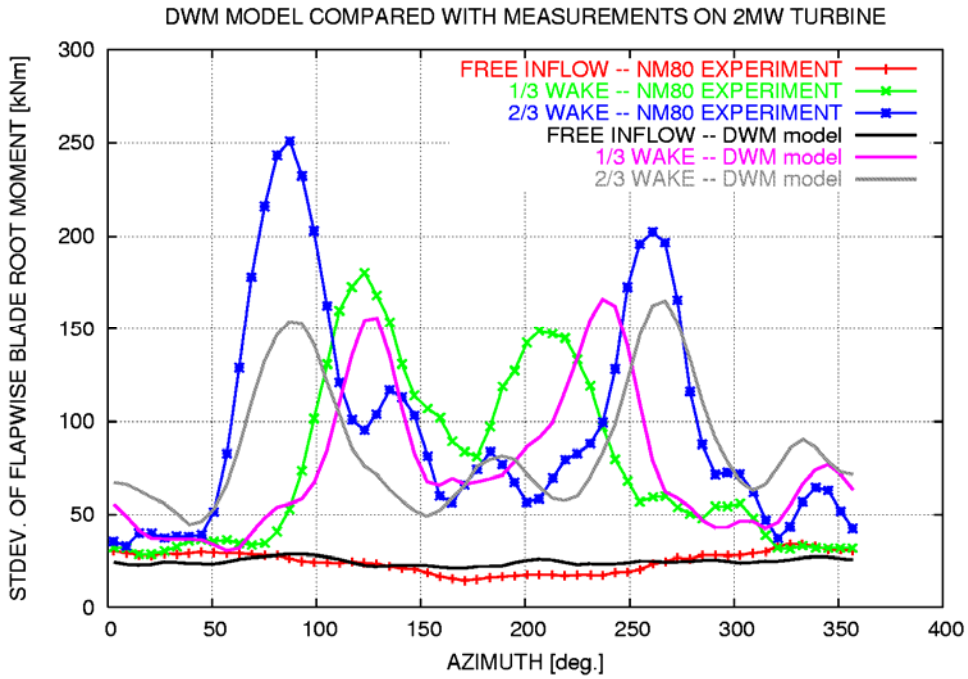

Figure 3-3 Comparison of root mean squares of the flapwise root moment as simulated with the DWM model and obtained from full scale measurements, respectively.

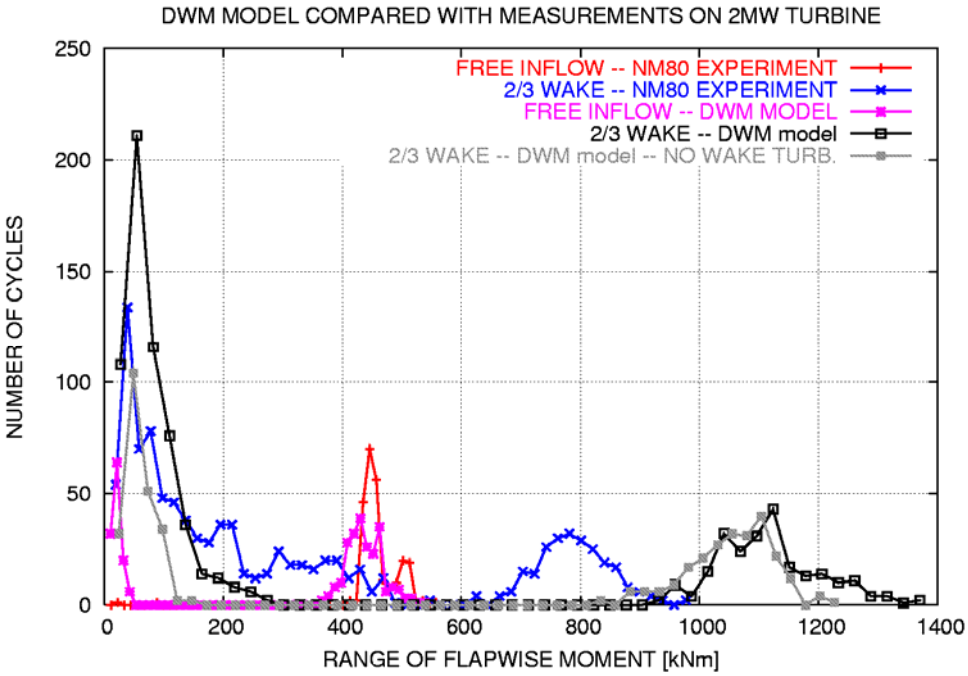

Figure 3-4 Comparison of rainflow counting results, corresponding to the flapwise root moment, as based on DWM model predictions and full scale measurements, respectively.

As seen in Figure 3-1, Figure 3-2 and Figure 3-3 the investigated wake conditions occurred on the lower part of the rotor; centered around an azimuth angle of approximately 180 deg. The flow cases selected for the analysis represent free inflow as well as partial wake inflow conditions (i.e. approximately 1/3 and 2/3 wake conditions). In the simulation of these load cases the turbine was modeled with normal flexibility of the turbine structure.

Overall, there is a good correlation between the DWM predictions and the full scale measurements as concerns the root mean square of the investigated parameters binned with respect to the rotor azimuthal angle. As an example, the "double peek structure" in the root mean square of the flapwise moment is seen both in the simulations and in the measurements. The largest difference between the DWM model predictions and the full scale measurements is observed in the rainflow counting results of the flapwise moment, cf. Figure 3-4. The 2/3 wake condition causes considerably higher fatigue loads in the simulations as compared with the measurements. The difference seems to be caused by a less developed wake deficit in the experiment than computed with the DWM model. For the smaller fatigue cycles it seems that the added wake turbulence improves the correlation with experiment. However, the increase in fatigue loading, caused by the added wake turbulence, is only about 6% for the present case, thus confirming that the wake deficit meandering is the main additional fatigue load driver in wake situations.

Simulated and measured power spectral densities (PSD's) of the relative velocity and the flapwise root moment, respectively, are compared in Figure 3-5 and in Figure 3-6. The general correlation between the simulated and the measured PSD's is good. One simulation was made without added wake turbulence, and in this case the simulated spectrum of the relative velocity differs considerably from the measured contra part, thus giving confidence to the implemented simple model of added wake turbulence in the DWM framework.

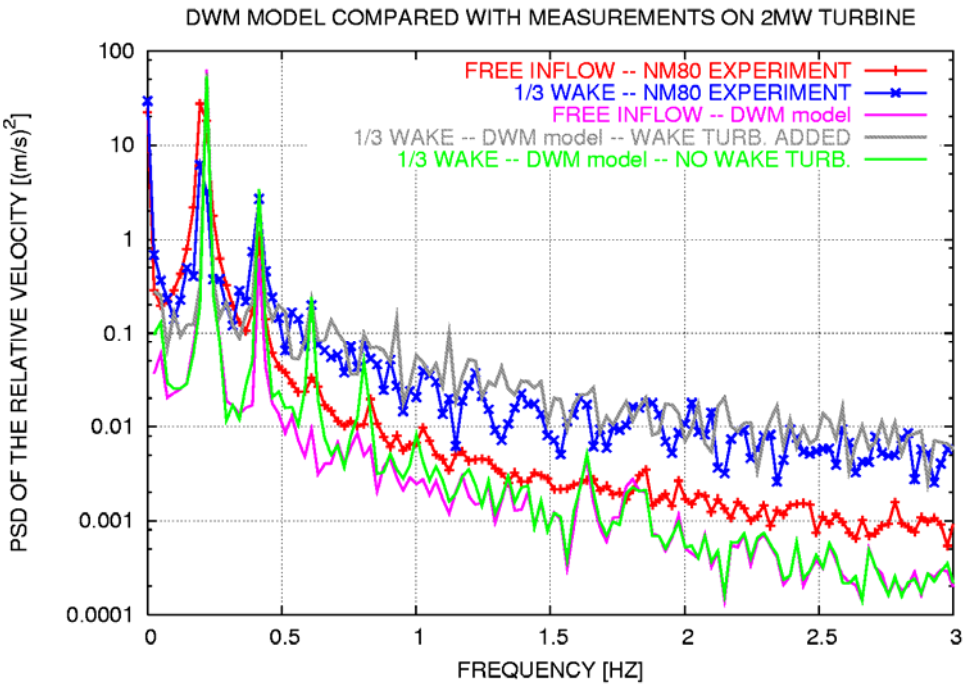

Figure 3-5 PSD spectra of the relative velocity for free inflow and for 1/3 wake operation, respectively, computed with the DWM model and extracted from experiment.

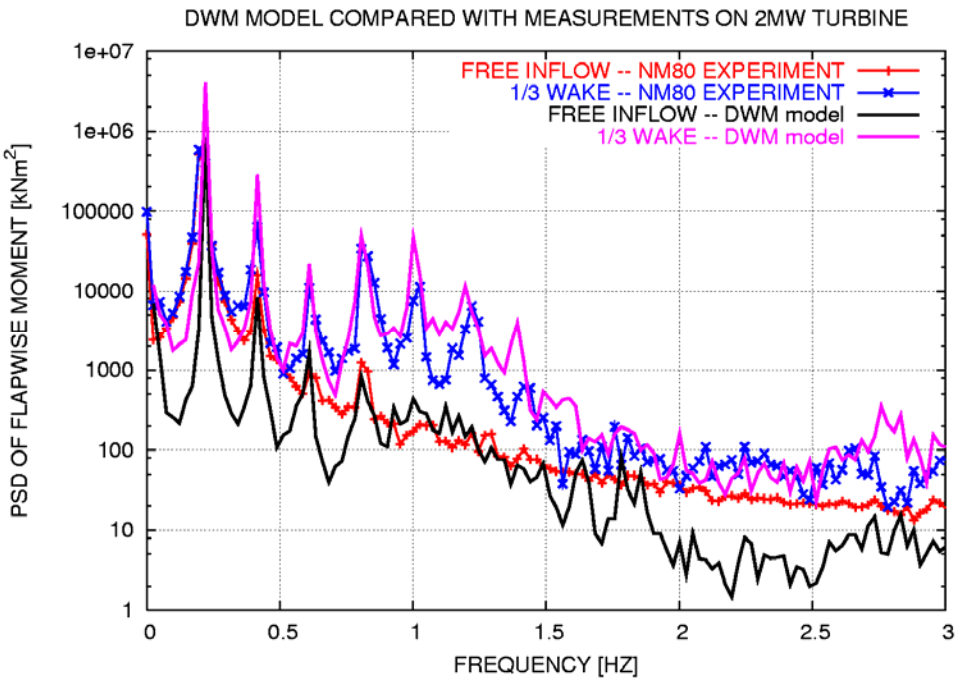

Figure 3-6 PSD spectra of the flapwise root moment for free inflow and for 1/3 wake operation, respectively, computed with the DWM model and extracted from experiment.

The performance of the implemented added wake turbulence model is further illustrated in Figure 3-7 and Figure 3-8, where the character of local inflow angle time series, with and without added wake turbulence contributions, is shown for DWM predictions and for measurements, respectively. As for the experimental data, the situation without added wake turbulence is obtained from the free inflow condition case. The very "regular" appearance of the local inflow angle as function of time for the free inflow condition is due to the very low ambient turbulence in this case. The low turbulence inflow is also true for the wake load case, which in turn means that the observed wake turbulence contribution can be considered as originating from added wake turbulence, because the meandering effect can be neglected under such circumstances.

The influence from added wake turbulence is seen as small ripples in the angle of attack, when the blade enters the (partial) wake load situation. These ripples contribute to small load cycles in the blade fatigue loading. As seen the character of these ripples are qualitative very similar for the DWM predictions and for the experiment data, respectively.

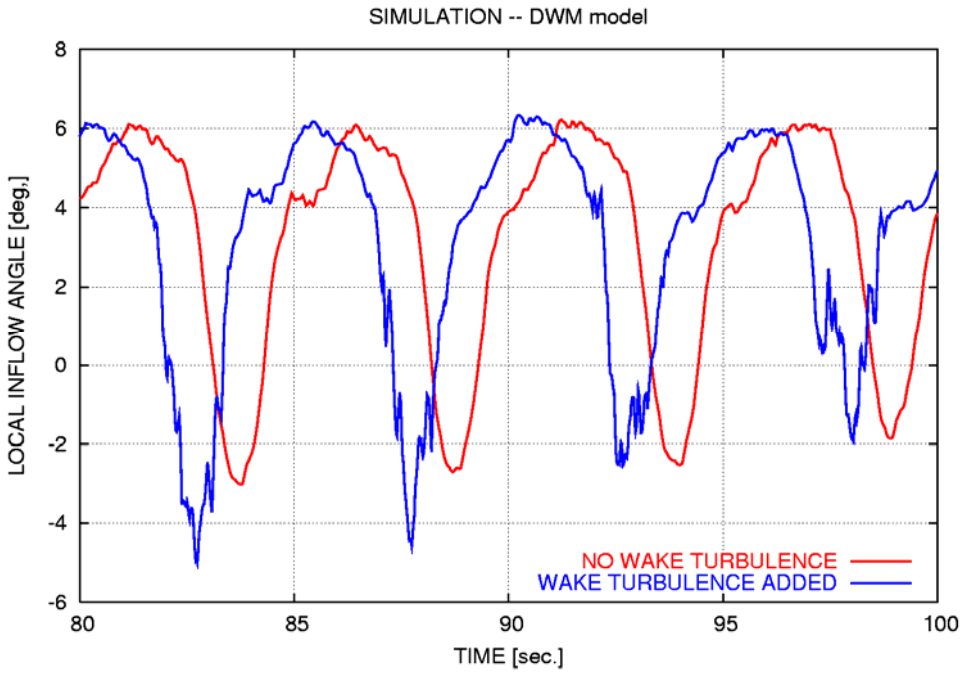

Figure 3-7 Effect from added wake turbulence on the simulated local inflow angle. Added wake turbulence causes small ripples in angle of attack, when the blade is in the wake loaded area.

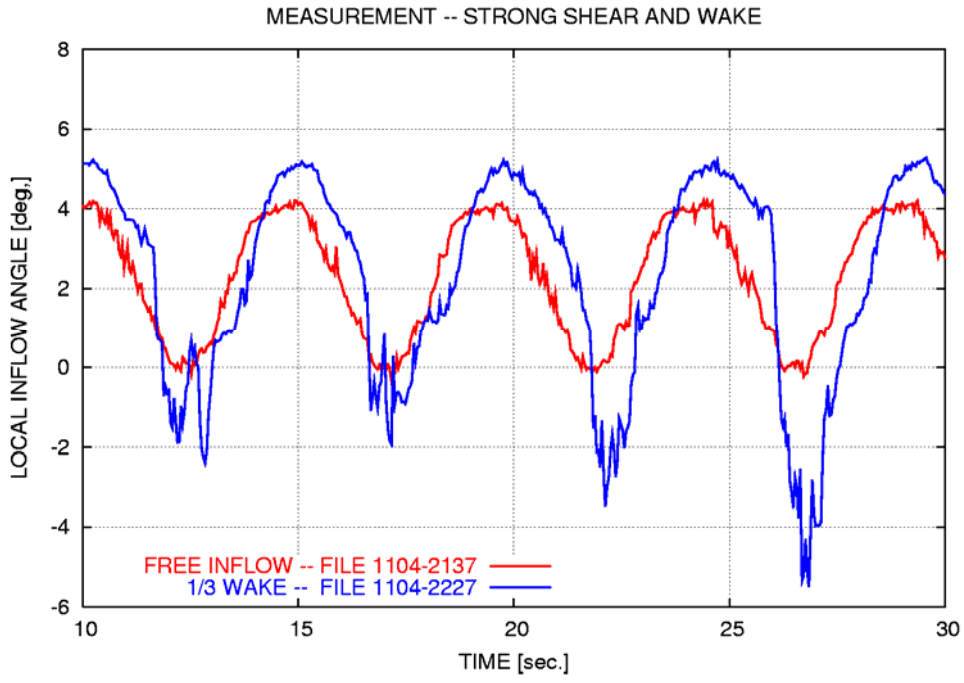

Figure 3-8 Effect from added wake turbulence on the measured local inflow angle. Added wake turbulence causes small ripples in angle of attack, when the blade is in the wake loaded area.

4 Conclusions

In the first versions of the DWM model the quasi-steady wake deficit was computed "externally", basically by interfacing a CFD actuator disc model with an aeroelastic model. Further, only the part of the increased wake turbulence caused by wake meandering was taking into account, whereas the added wake turbulence contribution was not included.

The DWM model has now been further developed primary by including models of the quasi-steady wake deficit and the added wake turbulence as integrated parts of the DWM model complex. Moreover the DWM model complex has been fully integrated in the aeroelastic model HAWC2.

The model of the quasi-steady wake deficit is based on the *thin shear layer approximation* of the rotationally symmetric Navier-Stokes equations. This formulation requires an initial wake deficit, which essentially is obtained from induced velocities in the rotor plane of the wake generating turbine determined from a BEM modeling. Wake expansion caused by both ambient turbulence and by the turbulence generated by the wake shear field itself is taken into account.

In a crude preliminary approach, the *in-homogeneous* added wake turbulence field is obtained in an approximate manner by *simple scaling* of a homogeneous turbulence field based on the Mann spectral tensor.

Predictions from the integrated DWM model complex have finally been analyzed and compared with existing full-scale measurements from the small Tjæreby wind farm.

The comparisons between DWM predictions and measurements have encompassed statistics of the wake flow field (local inflow angle, local relative velocity) as well as statistics of structural response (flapwise root bending moment), and in general a satisfactory agreement was found.

For the investigated case, the added wake turbulence increased the fatigue loading of the flapwise blade root moment with 6%, compared to wake load estimates with the added wake turbulence contribution excluded. This result supports the conjecture that the major additional load contribution in wake situations is due to the meandering of the quasi-steady wake deficit.

5 References

[1] Larsen, G.C., Madsen, H.Aa., Thomsen, K. and Larsen, T.J.. Wake meandering - a pragmatic approach. *Wind Energy* (2008) **11**, 377-395.

[2] Madsen, H.Aa., Larsen, G.C., Larsen, T.J., Mikkelsen, R., and Troldborg, N. (2008). Wake deficit-and turbulence simulated with two models compared with inflow measurements on a 2MW turbine in wake conditions. In: Scientific proceedings. 2008 European Wind Energy Conference and Exhibition, Brussels (BE), 31 Mar - 3 Apr 2008. p. 48-53.

[3] Larsen, G.C., Madsen, H.Aa., Bingöl, F., Mann, J., Ott, S., Sørensen, J.N., Okulov, V., Troldborg, N., Nielsen, M., Thomsen, K., Larsen, T.J., and Mikkelsen, R. (2007). Dynamic wake meandering modeling. Risø-R-1607(EN), 84 p. Risø National Laboratory for Sustainable Energy, Technical University of Denmark.

[4] Ainslie, J.F. (1985). Development of an eddy viscosity model for wind turbine wakes. In: Proceedings of the BWEA conference 1985, pp. 61-66.

[5] Ainslie, J.F. (1986). Wake modeling and the prediction of turbulence properties. Proceedings of the 8th British Wind energy Association Conference, Cambridge 19-21 March. pp. 115-120.

[6] Ainslie, J.F. (1988). Calculating the flow field in the wake of wind turbines. Journal of Wind Engineering and Industrial Aerodynamics, 27, pp. 213-224.

[7] Mann, J. (1998). Wind field simulation. Prob. Eng. Mech. **13**, 269-282.

[8] Bingöl, F., Larsen, G.C. and Mann, J. (2007). Wake meandering – an analysis of instantaneous 2-D laser measurements. The Second Conference on The Science of making Torque from Wind. 28-31 August, Technical University of Denmark. *J. Phys.: Conf. Ser.* (2007) **75**, 8 p.

[9] Mann, J. (1994). The Spatial Structure of Neutral Atmospheric Surface-Layer Turbulence. J. of Fluid Mech., 273, pp. 141-168.

[10] Troldborg, N., Sørensen, J.N and Mikkelsen, R. (2007). Actuator Line Simulations of Wake of Wind Turbines in Turbulent Inflow. In proceedings at EAWE PhD seminar, Pamplona, Spain, October, 2007.

[11] Nielsen, M., Larsen, G.C., and Hansen, K.S. (2007). Simulation of inhomogeneous, non-stationary and non-Gaussian turbulent winds. International conference: The science of making torque from wind, Lyngby (DK), 28-31 Aug 2007. J. Phys.: Conf. Ser. (2007) **75** , 9 p.

[12] Shinozuka, M. and Jan, C.M. (1972). Digital Simulation of random Processes and Its Applications. Journal of Sound and Vibration, Vol. 25. No. 1, pp. 111-128.

[13] Veers, P.S. (1988). Three Dimensional Wind Simulation. SAND88-0152, Sandia National Laboratories.

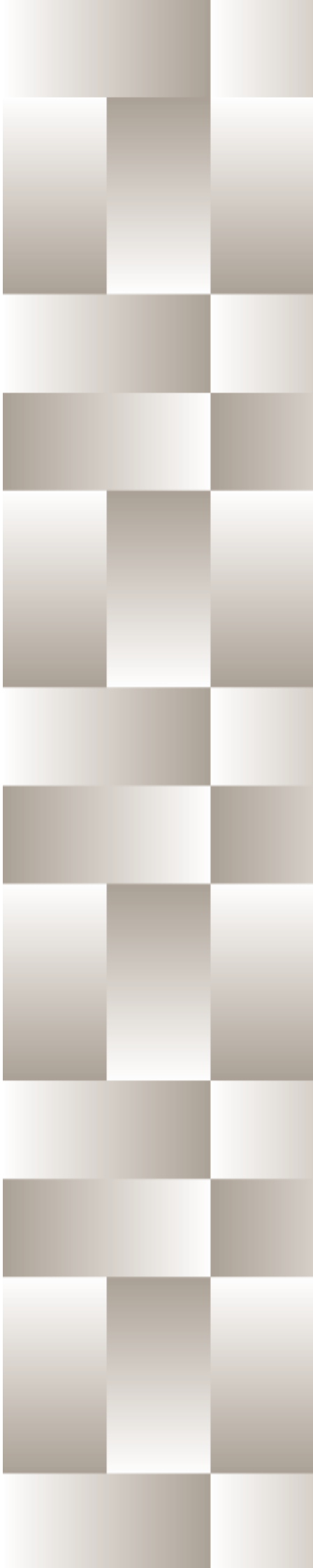

www.risoe.dk